(DOI: will be inserted by hand later)

Benchmarking atomic data for astrophysics: Fe XVIII

G. Del Zanna

University College London, MSSL, Holmbury St. Mary Dorking Surrey RH5 6NT UK

Received / Accepted

Abstract. Fe XVIII produces L-shell ($n = 2, 3, 4 \rightarrow 2$) spectral lines in the X-rays and extreme ultraviolet, which are among the brightest lines in e.g. solar flares and in Chandra, XMM-Newton spectra of active stars. The recent R-matrix scattering calculations of Witthoeft et al (2006) produce theoretical intensities for some of the brightest transitions increased by large factors (2-3), and is therefore timely to use these calculations to review and assess all previous line identifications on a quantitative basis. This paper discusses only the most important lines for laboratory and astrophysical applications. Many previous identifications are revised and some tentative ones are finally confirmed. Many lines are found to be significantly blended. A considerable number of new identifications is proposed. Excellent agreeement between observed and predicted intensities is found, for the first time, in the majority of cases. It is therefore now possible to use Fe XVIII L-shell lines to measure electron densities in laboratory plasmas and temperatures for a wide range of astrophysical sources.

Key words. Atomic data – Line: identification – Sun: corona – Techniques: spectroscopic

1. Introduction

This paper continues the series of benchmarks of the best atomic data against high-resolution spectra of laboratory and astrophysical sources. The main aim is to discuss line identifications and blends, suggest the best spectral lines to be used for plasma diagnostics, and provide some uncertainty estimates on the theoretical data. For a description of the general methods and goals see Paper I (Del Zanna et al. 2004).

Send offprint requests to: G. Del Zanna (gdz@mssl.ucl.ac.uk)

In this paper Fe XVIII L-shell ($n = 2, 3, 4 \rightarrow 2$) emission is considered. This emission is prominent in solar flare spectra (see, e.g., Neupert et al. 1967), and in laboratory plasmas (see, e.g., Boiko et al. 1978). Fe XVIII is very abundant (in ionization equilibrium) at temperatures $T \simeq 5$ MK (1 MK=10^6 K), close to the typical temperatures of many active stellar coronae (e.g. Capella, 6 MK). Fe XVIII lines are therefore among the strongest ones in XUV spectra of active stars, as Chandra, XMM-Newton and EUVE observations have shown.

Previous scattering calculations on this ion were based on distorted-wave (DW) approximations (e.g. Mann 1983, Cornille et al. 1992, Sampson et al. 1991). Commonly-used spectral codes or atomic databases (e.g. ATOMDB, SPEX) were based on these types of calculations. For example, ATOMDB (previously known as APEC) included collisional data obtained with HULLAC, widely used in the astrophysical community. As shown in Witthoeft et al. (2006) (hereafter W06) with some examples, models based on these calculations largely underestimate the intensities for some of the strongest spectral lines, in particular for the $2s^2\ 2p^4\ 3s \rightarrow 2s^2\ 2p^5$ transitions. The discrepancies between observed and modelled spectra have been so large that in many previous papers these lines were listed as only tentatively identified. Similar discrepancies persisted with the limited R-matrix calculation of Mohan et al. (1987). Desai et al (2005) recently showed that large (factors of two) discrepancies also occurr for the Capella spectrum, even when more recent calculations based on the FAC code are used. Notice that Capella is the brightest star in the X-rays.

The first complete R-matrix calculation including all resonances up to $n = 4$ has been performed recently by W06 as part of the IRON Project collaboration. These new collision strengths are significantly different from the previous ones. In light of these results, it is therefore important to re-assess all previous line identifications by taking into account not only wavelength coincidences and oscillator strengths (as mostly done in the past literature), but especially line intensities. Notice that Fe XVIII L-shell emission falls in a spectral region densely packed with hundreds of transitions from different ionization stages of Iron and other elements, many of which are still either unidentified or have a questionable identification.

It has been known/suggested that Fe XVIII L-shell lines could be used to measure the electron temperatures of astrophysical sources (Cornille et al. 1992), or densities in laboratory plasmas, however these were not previously applied in the literature.

Sect. 2 describes the experimental data that have been used in the benchmark. Sect. 3 describes the procedures and the atomic data adopted. Sect. 4 presents the results while Sect. 5 draws the conclusions.

2. Observations of Fe XVIII lines

The first observations of $n = 3 \rightarrow 2$ Fe XVIII lines in solar flares were made with the OSO-III satellite which observed the 1.3–20 Å region and were reported by Neupert et al. (1967). Neupert et al. (1973) presented OSO-5 spectra of solar flares in the 6–25 Å region. They also contained strong Fe XVIII emission, but at the time no identifications were available. Kastner et al. (1974) reported the first solar flare spectra containing the $n = 2 \rightarrow 2$ L-shell iron emission, in the 66–171 Å range from OSO-5.

Some of the first identifications came from Fawcett et al. (1967). Many more identifications (and mis-identifications) followed. Some for the $2s^2\ 2p^4\ 3d \rightarrow 2s^2\ 2p^5$ transitions (herafter 3d-2p) came from the observations of low-inductance vacuum spark spectra reported by Cohen et al. (1968) (herafter Co68). Further revisions were produced by Feldman et al. (1973a) together with identifications of most of the strong $2s^2\ 2p^4\ 3s \rightarrow 2s^2\ 2p^5$ transitions (herafter 3s-2p). Approximate intensities were provided.

Later, a Nd-glass laser spectrum was produced by Chase et al. (1976). This spectrum proved to be very useful, because the strongest lines were from Fe XVIII and Fe XIX. Unfortunately the spectral resolution and wavelength calibration were not very good. However, this spectrum enabled Bromage et al. (1977a) to provide identifications of a few $2s^2\ 2p^4\ 4d \rightarrow 2s^2\ 2p^5$ transitions.

A much better laboratory spectrum for Fe XVIII was later produced by Bromage et al. (1977b) (hereafter Br77) using a high-power neodyum glass laser and crystal spectrographs. Many more weaker lines were observed, and approximate line intensities provided. The further advantage of this spectrum was the lack of iron emission due to ionization stages higher than XXI and the excellent spectral resolution.

Laser spectra were also published in a series of papers (see Boiko et al. 1978 and references therein). The Boiko et al. (1978) spectral accuracy and resolution ($\simeq$0.002 Å on average) was excellent, and approximate line intensities, corrected for the film response and the filter absorption, were provided. One drawback of these spectra was the presence of emission lines of all ionization stages of iron. The laboratory plasmas had typical densities of the order of 10^{18}–10^{20} cm^{-3} and temperatures of the order of 10^7 K. At such high densities, many lower levels become significantly populated, and many line ratios become highly density-sensitive.

After the early solar observations, further improvements in terms of spectral resolution was achieved with the SOLEX spectrometers (see McKenzie et al. 1980, 1985), although the data lacked wavelength accuracy. The Solar Maximum Mission (SMM) flat crystal spectrometers (FCS) produced one solar flare spectrum of excellent quality (see Phillips et al. 1982). The main limitation of these solar observations was the fact that the spectral range was scanned, hence different lines were not observed simultaneously. This considerably complicates the analysis (cf. Landi & Phillips 2005).

Probably the best solar spectrum containing Fe XVIII lines was recorded during a rocket flight on July 13 1982 (Acton et al. 1985). The spectrograph was of excellent resolution (0.02 Å) and quality. Spectra in the 10–100 Å range were recorded on film, and later photometrically calibrated.

Recently, Electron Beam Ion Trap (EBIT) spectra containing the few brightest $n = 3 \rightarrow 2$ lines have been published by Brown et al. (2002). Compared to laser spectra, the advantage of tokamak and EBIT spectra is the low density (similar to that one of solar flares), and the presence of lines only from a restricted range of ions. The limitations of these laboratory data are the poor spectral resolution, the low signal-to-noise, and the lack of a radiometric calibration.

Further observations of Fe XVIII spectral lines with a resolution comparable to the best solar ones have been obtained with the Chandra high-energy transmission grating (HETG) for a variety of 'hot' astrophysical sources.

3. The benchmark method

The general procedures of the benchmark method are described in detail in Del Zanna et al. (2004), while specific issues related to high-density laser spectra are discussed in Del Zanna et al. (2005). In summary, steady-state optically-thin emission in a plasma collisionally ionised and excited mainly by electrons having a Maxwellian distribution is assumed. Even in laboratory spectra, the lifetimes of the excited states are normally much shorter than the timescales over which the plasma conditions vary, and steady-state is a reasonable assumption. Ionisation and recombination processes can affect some of the level populations and hence line intensities, but are a secondary effect.

The benchmark method follows an iterative procedure. Atomic structure calculations (using SUPERSTRUCTURE, see Eissner et al. 1974) are run, together with the 'term energy correction' (TEC) procedure (see, e.g. Zeippen et al. 1977; Nussbaumer & Storey 1978), to obtain empirically-adjusted fine-structure energies $E_{\rm SS}$ and spontaneous transition probabilities A_{ji}. The adjustements are done by matching preliminary identifications of the strongest lines in each configuration.

The A_{ji} values, together with the collisional data of W06, are then used to calculate the fractional population $N_j(N_{\rm e}, T_{\rm e})$ of the upper level j (relative to the total number density of the ion), as a function of electron temperature $T_{\rm e}$ and density $N_{\rm e}$, by taking into account all excitations, de-excitations, cascading in steady-state conditions. Proton excitation within the ground state as available in CHIANTI (Landi et al. 2006) has been applied.

The theoretical intensities (proportional to $N_j A_{ji}$) at different densities and temperatures are compared to the observed intensities $I_{\rm ob}$, by plotting the 'emissivity ratio curves':

$$F_{ji}(N_{\rm e}, T_{\rm e}) = C \ \frac{I_{\rm ob} N_{\rm e}}{N_j(N_{\rm e}, T_{\rm e})\ A_{ji}} \tag{1}$$

calculated at a fixed temperature $T_{\rm e} = T_0$ (or at a fixed density $N_{\rm e} = N_0$) as a function of the electron density $N_{\rm e}$ (or temperature $T_{\rm e}$). For the astrophysical spectra considered here, a fixed density 10^{10} cm^{-3} has been adopted. Notice that the emissivity ratios are virtually insensitive to densities up to 10^{12} cm^{-3}, typical of flare plasmas. Notice that in ionization equilibrium Fe XVIII has peak abundance at $T = 10^{6.6-6.8}$ K.

The proportionality constant C is chosen for each dataset so that the emissivity ratios are close to unity. If agreement between theory and observations holds, the F_{ji} values for different spectral lines should approximately overlap. The line identifications and wavelengths are adjusted and the procedure is repeated in order to identify all the spectral lines that should be observable and provide a set of best energies $E_{\rm best}$. These energies are the adjusted observed energies $E_{\rm obs}$, whenever available, and the adjusted $E_{\rm SS}$ values otherwise.

This method is equivalent to the widely-used line ratio one, but has the advantage of providing an overall view for all the spectral lines at once. It also clearly shows which combination of lines can be used for density and temperature diagnostics. Notice that if the emitting plasma is isothermal, the emissivity ratio curves provide a direct way to measure electron temperatures.

The benchmark method adopted here is approximate, but at least is more refined than a simple use of weighted absorption oscillator strengths (gf values), widely adopted for line identification. The key for line identification is to calculate theoretical spectra at different regimes, and start identifying the brightest lines first. High-density laboratory spectra have provided most line identifications, but most line ratios change dramatically once in the low-density regime in astrophysical plasmas. This might be the reason why mis-identifications are common in the literature.

4. Results

Table 1 lists the set of adopted configurations to calculate the radiative data in intermediate coupling. These configurations give rise to 279 fine-structure levels and are the same used in W06, in order to make sure of proper level assignements. TECs of the order of 10000 cm^{-1} have been applied to most configurations. The application of TECs resulted in the change of the ordering of just a few levels. For the levels for which no observed energy could firmly be established an energy correction of 10000-12000 cm^{-1} was applied.

Table 1. The configurations used to calculate the energy levels and the radiative data.

c1: $2s^2\ 2p^5$	c2: $2s\ 2p^6$	c3: $2s^2\ 2p^4\ 3s$	c4: $2s^2\ 2p^4\ 3p$
c5: $2s^2\ 2p^4\ 3d$	c6: $2s\ 2p^5\ 3s$	c7: $2s\ 2p^5\ 3p$	c8: $2s\ 2p^5\ 3d$
c9: $2s^2\ 2p^4\ 4s$	c10: $2p^6\ 3s$	c11: $2s^2\ 2p^4\ 4p$	c12: $2s^2\ 2p^4\ 4d$
c13: $2p^6\ 3p$	c14: $2s^2\ 2p^4\ 4f$	c15: $2p^6\ 3d$	c16: $2s\ 2p^5\ 4s$
c17: $2s\ 2p^5\ 4p$	c18: $2s\ 2p^5\ 4d$	c19: $2s\ 2p^5\ 4f$	c20: $2p^6\ 4s$
c21: $2p^6\ 4p$	c22: $2p^6\ 4d$	c23: $2p^6\ 4f$	

Table 2 presents a summary of the best energies $E_{\rm best}$ compared to the energies available from the NIST database v.3[1] for the configurations that are providing observed spectral lines. The ordering of the levels is the same as in the scattering calculation. We note good agreement (mostly within uncertainties) between many observed energies and the NIST ones. However, notable exceptions are present. Many new energy levels are proposed here.

The A values have been calculated with SUPERSTRUCTURE using the best energies. These values compare well (within 10%) with those previously available in the literature. In particular, with those of W06 and with the relativistic Hartree-Fock calculation of Fawcett (1984), which included semi-empirical corrections. Values for the brightest transitions are shown in the Appendix.

Unfortunately a lack of beam-foil spectroscopic measurements prevents a thorough check on A values. Buchet et al. (1980) measured the lifetime of the $2s\ 2p^6\ ^2S_{1/2}$ level to be 12.2±0.8 ps. This is to be compared with the value of 9.1 obtained here.

Table 3 provides a summary list of all the lines that are predicted to be brightest, at both low-densities (10^{12} cm^{-3}, astrophysical plasmas) and high-densities (10^{19} cm^{-3}, laser plasmas), with a list of identifications. The second and third columns give the relative intensities of the lines. The fourth column lists the wavelengths calculated from the best energies $E_{\rm best}$, while the fifth column lists our selection of best observed wavelengths λ_{obs}, with their uncertainties. All the lines observed in astrophysical plasmas have also been observed in laboratory, hence laboratory wavelengths are normally adopted here. The sixth column indicates some of the original identifications found in the literature. Note that clear assignments for original identifications are sometimes difficult to assess for a variety of reasons.

More details on new line identifications for each specific set of observations are to be found within the emissivity ratio plots. Each emissivity ratio plot shows, for each line: a comment on the identification (R: revised identification; N: new identification; bl: blend of more transitions; bl u: blend with an unidentified line); the observed intensity $I_{\rm ob}$

[1] http://physics.nist.gov/PhysRefData/ASD/index.html

Table 2. The details of some of the levels in the most important configurations in Fe XVIII. $E_{\rm best}$ indicates the best energies ($\rm cm^{-1}$) proposed here. The uncertainties in the energies reflect the estimated errors in the wavelength measurements. Levels with uncertain identification are assigned an uncertainty of 5000 $\rm cm^{-1}$. The following columns indicate the differences between our $E_{\rm best}$ and the energies from NIST $E_{\rm NIST}$ (v.3), and the collisional calculations $E_{\rm CC}$ of W06.

i	Conf. ($1s^2$)	Term	$E_{\rm best}$	$E_{\rm best}$-$E_{\rm NIST}$	$E_{\rm best}$-$E_{\rm CC}$
1	$2s^2$ 2p(99%)	$^2P^o_{3/2}$	0.0 ± 0	0	+0
2	$2s^2$ $2p^5$(99%)	$^2P^o_{1/2}$	102579.0 ± 1	0	-2253
3	2s $2p^6$(99%)	$^2S^e_{1/2}$	1064600.0 ± 100	-102	-14168
4	$2s^2$ $2p^4$ 3s(91%)	$^4P^e_{5/2}$	6222000.0 ± 1550	0	-10863
5	$2s^2$ $2p^4$ 3s(56%) +10(10%) +7(32%)	$^2P^e_{3/2}$	6248050.0 ± 1950	-50	-12662
6	$2s^2$ $2p^4$ 3s(83%) +16(14%)	$^4P^e_{1/2}$	6301200.0 ± 1590	-9000	-7814
7	$2s^2$ $2p^4$ 3s(66%) +5(31%)	$^4P^e_{3/2}$	6317900.0 ± 1600	0	-9955
8	$2s^2$ $2p^4$ 3s(89%)	$^2P^e_{1/2}$	6342600.0 ± 1500	0	-11113
9	$2s^2$ $2p^4$ 3s(91%)	$^2D^e_{5/2}$	6401200.0 ± 1200	1200	-12241
10	$2s^2$ $2p^4$ 3s(87%) +5(11%)	$^2D^e_{3/2}$	6403800.0 ± 1590	0	-13412
11	$2s^2$ $2p^4$ 3p(60%) +22(12%)	$^4P^o_{3/2}$	6458370.0 ± 5000	-	-18251
12	$2s^2$ $2p^4$ 3p(67%) +21(23%)	$^4P^o_{5/2}$	6462600.0 ± 5000	-	-17712
13	$2s^2$ $2p^4$ 3p(21%) +19(40%) +38(19%) +23(13%)	$^2P^o_{1/2}$	6488759.0 ± 5000	-	-18248
14	$2s^2$ $2p^4$ 3p(90%)	$^4D^o_{7/2}$	6494300.0 ± 5000	-	-18607
15	$2s^2$ $2p^4$ 3p(60%) +25(10%) +21(14%) +12(13%)	$^2D^o_{5/2}$	6494900.0 ± 5000	-	-19626
16	$2s^2$ $2p^4$ 3s(77%) +6(11%)	$^2S^e_{1/2}$	6550900.0 ± 1700	-24200	-12106
29	$2s^2$ $2p^4$ 3p(47%) +20(41%)	$^2P^o_{3/2}$	6739400.0 ± 1300	-	-19290
30	$2s^2$ $2p^4$ 3p(29%) +13(14%) +38(45%)	$^2P^o_{1/2}$	6759154.0 ± 5000	-	-18010
31	$2s^2$ $2p^4$ 3d(73%)	$^4D^e_{5/2}$	6804316.0 ± 5000	-	-11854
32	$2s^2$ $2p^4$ 3d(76%) +45(16%)	$^4D^e_{7/2}$	6805798.0 ± 5000	-	-11898
33	$2s^2$ $2p^4$ 3d(63%) +40(16%)	$^4D^e_{3/2}$	6809090.0 ± 5000	-	-11822
34	$2s^2$ $2p^4$ 3d(49%) +39(19%) +42(16%) +58(13%)	$^4D^e_{1/2}$	6819082.0 ± 5000	-	-11783
35	$2s^2$ $2p^4$ 3p(78%)	$^2P^o_{3/2}$	6822301.0 ± 5000	-	-18204
36	$2s^2$ $2p^4$ 3d(89%) +51(10%)	$^4F^e_{9/2}$	6830970.0 ± 5000	-	-11854
37	$2s^2$ $2p^4$ 3d(58%) +50(12%) +45(26%)	$^2F^e_{7/2}$	6839870.0 ± 5000	-	-13417
38	$2s^2$ $2p^4$ 3p(11%) +30(46%) +13(34%)	$^2P^o_{1/2}$	6845322.0 ± 5000	-	-17821
39	$2s^2$ $2p^4$ 3d(64%) +42(19%)	$^4P^e_{1/2}$	6858700.0 ± 1000	500	-10530
40	$2s^2$ $2p^4$ 3d(50%) +46(25%)	$^4P^e_{3/2}$	6872400.0 ± 1900	0	-11913
41	$2s^2$ $2p^4$ 3d(27%) +44(23%) +49(19%) +47(21%)	$^2F^e_{5/2}$	6879000.0 ± 1000	-1400	-14309
42	$2s^2$ $2p^4$ 3d(30%) +34(46%) +58(16%)	$^2P^e_{1/2}$	6896892.0 ± 5000	-6308	-11820
43	$2s^2$ $2p^4$ 3d(78%)	$^4F^e_{3/2}$	6902700.0 ± 1000	-	-9528
44	$2s^2$ $2p^4$ 3d(51%) +59(11%) +47(19%)	$^4F^e_{5/2}$	6902700.0 ± 1000	-1000	-12080
45	$2s^2$ $2p^4$ 3d(52%) +37(26%) +32(18%)	$^4F^e_{7/2}$	6913179.0 ± 5000	-	-12424
46	$2s^2$ $2p^4$ 3d(20%) +33(27%) +57(10%) +40(19%) +48(10%)	$^2D^e_{3/2}$	6919000.0 ± 2000	0	-9856
47	$2s^2$ $2p^4$ 3d(43%) +41(37%)	$^4P^e_{5/2}$	6935300.0 ± 1000	-	-10716
48	$2s^2$ $2p^4$ 3d(49%) +55(20%)	$^2P^e_{3/2}$	6947000.0 ± 4000	-300	-12355
49	$2s^2$ $2p^4$ 3d(44%) +41(25%) +56(14%)	$^2D^e_{5/2}$	6957500.0 ± 1000	0	-12530
50	$2s^2$ $2p^4$ 3d(85%)	$^2G^e_{7/2}$	6987191.0 ± 5000	-	-12627
51	$2s^2$ $2p^4$ 3d(89%) +36(10%)	$^2G^e_{9/2}$	6991759.0 ± 5000	-	-12275
52	$2s^2$ $2p^4$ 3d(62%) +56(26%)	$^2F^e_{5/2}$	7013600.0 ± 1000	-	-15252
53	$2s^2$ $2p^4$ 3d(83%)	$^2S^e_{1/2}$	7013600.0 ± 1000	-700	-15738
54	$2s^2$ $2p^4$ 3d(89%)	$^2F^e_{7/2}$	7025363.0 ± 5000	-	-14964
55	$2s^2$ $2p^4$ 3d(66%) +48(19%)	$^2P^e_{3/2}$	7037900.0 ± 1000	-500	-16068
56	$2s^2$ $2p^4$ 3d(33%) +52(21%) +59(14%) +49(25%)	$^2D^e_{5/2}$	7040300.0 ± 1000	-500	-19693
57	$2s^2$ $2p^4$ 3d(69%) +46(25%)	$^2D^e_{3/2}$	7070000.0 ± 4000	3900	-14390
58	$2s^2$ $2p^4$ 3d(59%) +42(33%)	$^2P^e_{1/2}$	7074100.0 ± 3000	-100	-17443
59	$2s^2$ $2p^4$ 3d(61%) +56(19%)	$^2D^e_{5/2}$	7162300.0 ± 3000	-4100	-9703
60	2s $2p^5$ 3s(98%)	$^4P^o_{5/2}$	7161204.0 ± 5000	-24596	-15169
61	$2s^2$ $2p^4$ 3d(61%) +46(14%)	$^2D^e_{3/2}$	7182700.0 ± 1000	-1600	-9737
62	2s $2p^5$ 3s(68%) +64(28%)	$^4P^o_{3/2}$	7197414.0 ± 1880	-386	-15166
63	2s $2p^5$ 3s(82%) +65(13%)	$^4P^o_{1/2}$	7242722.0 ± 5000	18122	-15252
64	2s $2p^5$ 3s(69%) +62(27%)	$^2P^o_{3/2}$	7250524.0 ± 1530	-376	-16426
69	2s $2p^5$ 3p(41%) +79(11%) +75(10%) +72(27%)	$^4D^e_{3/2}$	7449300.0 ± 2500	-15100	-12668
70	2s $2p^5$ 3p(50%) +74(47%)	$^2D^e_{5/2}$	7464400.0 ± 2500	-12800	-10428
71	2s $2p^5$ 3p(48%) +76(32%) +73(16%)	$^4D^e_{1/2}$	7476930.0 ± 5000	-	-11995
72	2s $2p^5$ 3p(60%) +69(36%)	$^2P^e_{3/2}$	7487800.0 ± 2200	0	-14694
73	2s $2p^5$ 3p(54%) +76(12%) +80(19%)	$^2P^e_{1/2}$	7508100.0 ± 3300	0	-12079
74	2s $2p^5$ 3p(32%) +67(39%) +70(23%)	$^4P^e_{5/2}$	7508100.0 ± 3300	0	-13597
75	2s $2p^5$ 3p(45%) +79(41%)	$^4P^e_{3/2}$	7513866.0 ± 5000	-16034	-11988
76	2s $2p^5$ 3p(51%) +71(44%)	$^4P^e_{1/2}$	7519602.0 ± 5000	-	-11828
77	2s $2p^5$ 3s(96%)	$^2P^o_{3/2}$	7537200.0 ± 5000	-	-7556
78	2s $2p^5$ 3s(93%)	$^2P^o_{1/2}$	7537200.0 ± 5000	-	-13931
79	2s $2p^5$ 3p(44%) +69(17%) +75(23%) +72(10%)	$^2D^e_{3/2}$	7558606.0 ± 5000	-8394	-11942
80	2s $2p^5$ 3p(58%) +73(25%)	$^2S^e_{1/2}$	7579774.0 ± 5000	-19626	-16413

Table 2. Contd.

i	Conf. ($1s^2$)	Term	$E_{\rm best}$	$E_{\rm best}$-$E_{\rm NIST}$	$E_{\rm best}$-$E_{\rm CC}$
81	2s $2p^5$ 3d(97%)	$^4P^o_{1/2}$	7713983.0 ± 5000	-	-21337
82	2s $2p^5$ 3d(87%) +97(11%)	$^4P^o_{3/2}$	7723705.0 ± 5000	-	-21298
83	2s $2p^5$ 3d(99%)	$^4F^o_{9/2}$	7733985.0 ± 5000	-	-21198
84	2s $2p^5$ 3d(60%) +94(30%)	$^4P^o_{5/2}$	7739843.0 ± 5000	-	-21226
85	2s $2p^5$ 3d(76%) +96(17%)	$^4F^o_{7/2}$	7743887.0 ± 5000	-	-21188
86	2s $2p^5$ 3d(54%) +95(15%) +84(16%)	$^4F^o_{5/2}$	7764578.0 ± 5000	-	-21145
87	2s $2p^5$ 3p(90%)	$^2D^e_{3/2}$	7775030.0 ± 5000	11630	-12279
88	2s $2p^5$ 3d(52%) +96(45%)	$^2F^o_{7/2}$	7780426.0 ± 5000	-	-20951
89	2s $2p^5$ 3d(54%) +97(22%) +99(15%)	$^4F^o_{3/2}$	7781809.0 ± 5000	-	-21113
90	2s $2p^5$ 3p(95%)	$^2D^e_{5/2}$	7801500.0 ± 3000	17600	-7933
91	2s $2p^5$ 3p(94%)	$^2P^e_{1/2}$	7805938.0 ± 5000	19938	-12115
92	2s $2p^5$ 3p(91%)	$^2P^e_{3/2}$	7816324.0 ± 5000	21924	-11982
93	2s $2p^5$ 3d(91%)	$^4D^o_{1/2}$	7811419.0 ± 5000	-	-21003
94	2s $2p^5$ 3d(47%) +101(28%) +84(14%)	$^4D^o_{5/2}$	7825043.0 ± 5000	-	-20947
95	2s $2p^5$ 3d(60%) +86(22%) +101(11%)	$^2D^o_{5/2}$	7825155.0 ± 5000	-	-20956
96	2s $2p^5$ 3d(35%) +85(21%) +88(40%)	$^4D^o_{7/2}$	7826259.0 ± 5000	-	-20937
97	2s $2p^5$ 3d(63%) +89(23%)	$^4D^o_{3/2}$	7832855.0 ± 5000	-	-21033
98	2s $2p^5$ 3p(77%) +80(18%)	$^2S^e_{1/2}$	7845790.0 ± 5000	-	-11307
99	2s $2p^5$ 3d(60%) +89(18%) +102(16%)	$^2D^o_{3/2}$	7834270.0 ± 1800	-	-25658
100	2s $2p^5$ 3d(86%) +106(10%)	$^2P^o_{1/2}$	7864650.0 ± 1800	-	-21603
101	2s $2p^5$ 3d(48%) +94(15%) +95(21%)	$^2F^o_{5/2}$	7876718.0 ± 5000	-	-20840
102	2s $2p^5$ 3d(74%) +99(17%)	$^2P^o_{3/2}$	7923400.0 ± 1000	-	-21201
103	2s $2p^5$ 3d(92%)	$^2F^o_{5/2}$	8103625.0 ± 5000	-	-20996
104	2s $2p^5$ 3d(96%)	$^2F^o_{7/2}$	8106455.0 ± 5000	-	-20963
105	2s $2p^5$ 3d(87%)	$^2P^o_{3/2}$	8118335.0 ± 5000	-	-20660
106	2s $2p^5$ 3d(86%)	$^2P^o_{1/2}$	8126521.0 ± 5000	-	-20574
107	2s $2p^5$ 3d(89%)	$^2D^o_{3/2}$	8133315.0 ± 5000	-	-20821
108	2s $2p^5$ 3d(94%)	$^2D^o_{5/2}$	8134038.0 ± 5000	-	-20839
109	$2s^2$ $2p^4$ 4s(90%)	$^4P^e_{5/2}$	8419134.0 ± 5000	-	-13174
110	$2s^2$ $2p^4$ 4s(70%) +122(10%) +113(19%)	$^2P^e_{3/2}$	8428196.0 ± 5000	-4	-13117
112	$2s^2$ $2p^4$ 4s(72%) +161(18%)	$^4P^e_{1/2}$	8493379.0 ± 5000	-	-13177
113	$2s^2$ $2p^4$ 4s(79%) +110(20%)	$^4P^e_{3/2}$	8507584.0 ± 5000	-9616	-13063
114	$2s^2$ $2p^4$ 4s(83%) +112(14%)	$^2P^e_{1/2}$	8514808.0 ± 5000	-	-13020
121	$2s^2$ $2p^4$ 4s(90%)	$^2D^e_{5/2}$	8591781.0 ± 5000	681	-13023
122	$2s^2$ $2p^4$ 4s(89%)	$^2D^e_{3/2}$	8592963.0 ± 5000	-37	-13012
130	$2s^2$ $2p^4$ 4d(62%) +157(12%) +163(14%)	$^4D^e_{5/2}$	8644764.0 ± 5000	-	-13713
131	$2s^2$ $2p^4$ 4d(65%) +160(25%)	$^4D^e_{7/2}$	8645002.0 ± 5000	-	-13602
132	$2s^2$ $2p^4$ 4d(31%) +162(47%)	$^4P^e_{3/2}$	8646812.0 ± 5000	-	-13743
133	$2s^2$ $2p^4$ 4d(16%) +159(28%) +136(43%) +182(10%)	$^2P^e_{1/2}$	8650636.0 ± 5000	-	-13694
134	$2s^2$ $2p^4$ 4d(90%)	$^4F^e_{9/2}$	8652211.0 ± 5000	-	-13516
135	$2s^2$ $2p^4$ 4d(68%) +174(10%) +160(18%)	$^2F^e_{7/2}$	8656340.0 ± 5000	-	-13463
136	$2s^2$ $2p^4$ 4d(39%) +133(42%)	$^4P^e_{1/2}$	8665274.0 ± 5000	-	-13367
137	$2s^2$ $2p^4$ 4d(31%) +132(32%) +165(20%)	$^2D^e_{3/2}$	8676800.0 ± 1500	800	-11603
138	$2s^2$ $2p^4$ 4d(39%) +164(23%) +163(18%)	$^2D^e_{5/2}$	8676800.0 ± 1500	800	-13988
156	$2s^2$ $2p^4$ 4d(57%) +162(13%) +196(15%)	$^4F^e_{3/2}$	8723045.0 ± 5000	-4455	-13476
157	$2s^2$ $2p^4$ 4d(45%) +130(21%) +195(13%) +163(14%)	$^4F^e_{5/2}$	8725894.0 ± 5000	-1606	-13454
159	$2s^2$ $2p^4$ 4d(66%) +133(22%)	$^4D^e_{1/2}$	8732590.0 ± 5000	-	-13500
160	$2s^2$ $2p^4$ 4d(51%) +135(20%) +131(28%)	$^4F^e_{7/2}$	8737085.0 ± 5000	-	-13428
161	$2s^2$ $2p^4$ 4s(76%) +112(12%)	$^2S^e_{1/2}$	8739122.0 ± 5000	-	-13216
162	$2s^2$ $2p^4$ 4d(30%) +156(18%) +137(13%) +132(22%) +165(11%)	$^4D^e_{3/2}$	8740345.0 ± 5000	-	-13340
163	$2s^2$ $2p^4$ 4d(43%) +157(14%) +164(32%)	$^4P^e_{5/2}$	8744662.0 ± 5000	-11938	-13326
164	$2s^2$ $2p^4$ 4d(33%) +157(12%) +138(46%)	$^2F^e_{5/2}$	8756600.0 ± 3000	-	-10829
165	$2s^2$ $2p^4$ 4d(50%) +137(28%)	$^2P^e_{3/2}$	8759800.0 ± 3500	-100	-11409
174	$2s^2$ $2p^4$ 4d(87%)	$^2G^e_{7/2}$	8817155.0 ± 5000	-	-13432
175	$2s^2$ $2p^4$ 4d(90%)	$^2G^e_{9/2}$	8819047.0 ± 5000	-	-13399
176	$2s^2$ $2p^4$ 4d(53%) +180(28%) +195(10%)	$^2D^e_{5/2}$	8829200.0 ± 3000	0	-11171
177	$2s^2$ $2p^4$ 4d(75%) +182(15%)	$^2S^e_{1/2}$	8827654.0 ± 5000	-1546	-13594
178	$2s^2$ $2p^4$ 4d(87%)	$^2P^e_{3/2}$	8829200.0 ± 3000	0	-14240
179	$2s^2$ $2p^4$ 4d(89%)	$^2F^e_{7/2}$	8831094.0 ± 5000	-	-13265
180	$2s^2$ $2p^4$ 4d(59%) +176(22%)	$^2F^e_{5/2}$	8829200.0 ± 3000	0	-17404
181	$2s^2$ $2p^4$ 4d(75%) +137(13%)	$^2D^e_{3/2}$	8842300.0 ± 1500	-1600	-14545
182	$2s^2$ $2p^4$ 4d(67%) +133(17%) +177(13%)	$^2P^e_{1/2}$	8842300.0 ± 1500	-1600	-17941
195	$2s^2$ $2p^4$ 4d(66%) +176(12%)	$^2D^e_{5/2}$	8972474.0 ± 5000	-	-13200
196	$2s^2$ $2p^4$ 4d(66%)	$^2D^e_{3/2}$	8989100.0 ± 3000	-100	-2203

(scaled original units); the lower and upper level indices (cf. Table 2) and the theoretical wavelengths of the main lines contributing to the observed one.

4.1. 3d→2p transitions

3d→2p transitions provide good diagnostics to measure electron densities in laboratory plasmas. Some of the original identifications of the brightest lines are due to Fawcett et al. (1967), Cohen et al. (1968) and Feldman et al. (1973). Fig. 1 shows the emissivity ratio curves based on the intensities of Feldman et al. (1973). Note that many lines are clearly blended, and many identifications have been revised.

Fig. 2 shows the emissivity ratio curves relative to the main 3d→2p transitions observed in the laser spectra by Boiko et al. (1978). The agreement between theory and observations is very good (within ±30%), considering the large uncertainties in the line intensities. Notice that in this and following cases some of the observed intensities have been reduced in order to take into account blending. The curves consistently indicate log $N_{\rm e}\simeq 20$ cm^{-3}. Quite good agreement is also found in the case of the Chase et al. spectra, shown in Fig. 3 (notice that many line identifications have been revised). In the case of the Bromage et al. (1977) spectrum, the agreement is surprisingly good (see Fig. 4), considering that intensities were just estimates based on the density of the emulsion.

All these different datasets provide similar results, i.e. that many lines are blended and/or were not identified correctly. The amount of blending is often consistent, which gives confidence in the results, considering the large variety of sources examined. One puzzling aspect is the low observed intensity of the strongest line, which must be a self-blend of the ^{2}P$_{3/2}$-^{2}D$_{5/2}$ (1-56) and the ^{2}P$_{3/2}$-^{2}P$^{\rm e}_{3/2}$ (1-55) transitions (a blend normally not reported in the literature). These two lines are espected to be very close in wavelength, and indeed in the highest-resolution spectra the observed line is wide. It is therefore possible that due to its large strength and width the intensity of this line has been underestimated. The same situation occurs also in some (but not all) of the astrophysical spectra examined.

In most of the solar flare or astrophysical plasmas, Fe XVIII emission is expected to be close to the low-density limit, and most of the lines observed in laboratory plasmas will not be detectable anymore.

To shed some light into the brightest lines observable in astrophysical plasmas, we consider now (Fig. 5) the rocket flight spectrum of Acton et al. (1985). Some of the lines that appear to be blended in laboratory spectra are still blended in the solar one (e.g. 1-59, 2-55+1-47), while others become blended (e.g. 2-61, 2-57, 1-41). The rest (1-56+1-55, 1-49, 1-40) show excellent agreement between calibrated and computed intensities. Notice that the 14.772 Å line cannot be due to the 2-40 transition alone. Actually a much stronger transition (3-99) is probably blending. Still, further blending is present.

Table 3. Line identifications. The columns indicate: 1) the indexes corresponding to Table 2; 2) the relative intensities (in photons, at 10^{12}, 10^{19} cm^{-3}), scaled to the strong 1-56+1-55 14.204 Å blend, calculated at log T=6.8; 3) the best wavelengths with their uncertainties (values in mÅ); 4) observed wavelengths λ_{obs} with their uncertainties; some blends are indicated (bl=blend; bl u= blend with an unidentified line); lines with no or a tentative identification have a question mark; 5) some of the previous original identifications; 6) some of the different identifications. Bo70: Boiko et al. (1970); Bo78: Boiko et al. (1978); Br77a: Bromage et al. (1977a); Br77: Bromage et al. (1977b); Co68: Cohen et al. (1968); Co92: Cornille et al. (1992); Dere78: Dere (1978); Do75: Doschek et al. (1975); Fa67:Fawcett et al. (1967); Fe73: Feldman et al. (1973a); Fe73b: Feldman et al. (1973b); P84: Peacock et al. (1984)

i-j	Int 10^{12}	Int 10^{19}	$\lambda_{\rm best}$(Å)	$\lambda_{\rm obs}$(Å)	same ID	diff. ID
2-196	1.6 10^{-3}	1.8 10^{-2}	11.253(4)	11.253(4) (bl u)	Br77a	
1-178	3.1 10^{-2}	2.9 10^{-2}	11.326(4)	11.326(4) Br77 (bl)	Br77a	
1-180	3.6 10^{-2}	2.9 10^{-2}	11.326(4)	11.326(4) Br77 (bl)	Br77a	
1-177	2.1 10^{-2}	1.8 10^{-2}	11.328(6)	11.326(4) Br77 (bl)	Br77a	
1-164	5.8 10^{-2}	4.3 10^{-2}	11.420(4)	11.420(4) Br77 (bl?)	Br77a	
2-181	9.7 10^{-3}	2.8 10^{-2}	11.442(2)	11.442(2) Bo78 (bl)	Br77	
2-182	5.7 10^{-3}	2.4 10^{-2}	11.442(2)	11.442(2) Bo78 (bl)	Br77	
2-178	7.6 10^{-3}	6.9 10^{-3}	11.459(4)	11.458(4) Br77 (bl u)		
1-137	3.0 10^{-2}	2.4 10^{-2}	11.525(2)	11.525(2) Bo78 (bl)	Br77a	
1-138	5.4 10^{-2}	4.2 10^{-2}	11.525(2)	11.525(2) Bo78 (bl)	Br77a	Bo78
2-165	4.9 10^{-3}	1.6 10^{-2}	11.551(5)	11.551(5) Br77 (bl u)	Br77 (R)	
1-90	1.1 10^{-2}	2.8 10^{-2}	12.818(5)	? 12.818(5) Br77 (bl Fe XX)		
1-73	1.2 10^{-2}	1.5 10^{-2}	13.319(6)	13.319(6) Br77 (bl)	Br77	
1-74	2.4 10^{-2}	4.8 10^{-2}	13.319(6)	13.319(6) Br77 (bl)	Br77	
1-72	1.9 10^{-2}	3.1 10^{-2}	13.355(4)	13.355(4) Br77	Br77	
2-80	3.4 10^{-3}	1.3 10^{-2}	13.374(9)	? 13.374(4) Br77 (bl u)		Br77
1-70	3.4 10^{-2}	5.4 10^{-2}	13.397(4)	13.397(4) Br77 (bl ?)		Br77
1-69	1.8 10^{-2}	2.6 10^{-2}	13.424(5)	13.424(4) Br77 (bl Fe XIX?)		Br77
1-67	1.9 10^{-2}	4.3 10^{-2}	13.464(5)	13.464(4) Br77 (bl Fe XIX ?)	Br77	
1-59	4.1 10^{-2}	5.9 10^{-2}	13.962(6)	13.962(2) Bo78 (bl u)	Co68,Fe73,Br77(.956)	
2-61	1.4 10^{-2}	0.23	14.124(2)	14.124(2) Bo78	Co68,Fe73, Br77,Bo78	
1-57	2.4 10^{-2}	5.9 10^{-2}	14.144(8)	14.155(2) Bo78 (bl)	Fe73, Br77(.152), Bo78	
3-106	3.2 10^{-3}	1.3 10^{-2}	14.160(10)	? 14.155(2) Bo78 (bl)		
3-105	4.4 10^{-3}	2.3 10^{-2}	14.177(10)	? 14.155(2) Bo78 (bl)		
1-56	0.64	0.50	14.204(2)	14.204(2) Bo78 (bl)	Fa67,Fe73, Br77, Bo78	
1-55	0.36	0.31	14.209(2)	14.204(2) Bo78 (bl)	Co69	
1-52	5.6 10^{-2}	8.1 10^{-2}	14.258(2)	14.258(2) Bo78 (bl)	?	
1-53	0.15	0.13	14.258(2)	14.258(2) Bo78 (bl)	Fe73, Br77, Bo78	Co69
2-58	5.0 10^{-2}	0.16	14.344(6)	14.344(6) Br77	Br77	
2-57	7.9 10^{-2}	0.19	14.353(8)	? 14.351(2) Bo78	Bo78, Fe73,Br77(.360)	
1-49	0.25	0.22	14.373(2)	14.373(2) Bo78	Fa67,Co69,Fe73,Br77,Bo78	
1-48	5.6 10^{-3}	1.3 10^{-2}	14.395(8)	? 14.387(2) Bo78		
1-47	4.6 10^{-2}	7.6 10^{-2}	14.419(2)	14.419(2) Bo78 (bl u)		
2-55	5.5 10^{-2}	4.8 10^{-2}	14.419(2)	14.419(2) Bo78 (bl u)	Fe73,Br77	
1-46	2.4 10^{-2}	4.2 10^{-2}	14.453(4)	14.453(6) Br77 (bl u)		Co69, Br77
2-53	2.5 10^{-2}	2.2 10^{-2}	14.470(2)	? 14.469(6) Br77 (bl u)	Fe73	Br77
1-43	3.2 10^{-2}	4.5 10^{-2}	14.487(2)	14.487(2) Bo78 (bl u)		Fe73, Br77, Bo78
1-44	1.7 10^{-2}	9.4 10^{-3}	14.487(2)	14.487(2) Bo78 (bl u)		Fe73
1-41	0.19	0.19	14.537(2)	14.538(2) Bo78	? Fe73, Br77,Bo78	
1-40	9.6 10^{-2}	0.10	14.551(4)	14.551(4) Br77 (bl u)	Co69, Fe73, Br77, Bo78	
1-39	4.5 10^{-2}	5.0 10^{-2}	14.580(2)	14.580(2) Bo78 (bl)	Fe73, Br77, Bo78	
3-102	8.6 10^{-3}	3.8 10^{-2}	14.580(2)	14.580(2) Bo78 (bl)		
2-48	2.2 10^{-2}	5.0 10^{-2}	14.610(9)	14.610(4) Br77 (bl u)	Br77	
2-46	1.8 10^{-2}	3.1 10^{-2}	14.670(4)	14.668(2) Bo78 (bl Fe XIX)		Bo78
3-100	2.2 10^{-2}	2.3 10^{-2}	14.706(4)	14.706(4) Br77 (bl Fe XIX)		
2-40	1.2 10^{-2}	1.3 10^{-2}	14.771(4)	14.772(4) Br77 (bl N)	Fe73, Br77	
3-99	3.0 10^{-2}	2.7 10^{-2}	14.772(4)	14.772(4) Br77 (bl)		
1-16	3.9 10^{-3}	1.4 10^{-2}	15.265(4)	? 15.258(2) Fe73 (bl Fe XVII)		Fe73
3-77	2.8 10^{-2}	2.6 10^{-2}	15.450(12)	? 15.450(4) Br77 (bl)		
3-78	2.0 10^{-3}	1.6 10^{-2}	15.450(12)	? 15.450(4) Br77 (bl)		
2-16	1.5 10^{-2}	5.3 10^{-2}	15.508(4)	? 15.508(4) Bo78 (bl u)		Fe73, Br77(.491),Bo78
1-9	0.31	0.26	15.622(3)	15.622(2) Bo78	Fa67,Fe73,Br77, Bo78	
1-8	4.4 10^{-2}	4.6 10^{-2}	15.766(4)	15.766(4) Br77 (bl u)	Fe73, Br77	
1-7	0.20	0.16	15.828(4)	15.828(4) Br77	Fa67,Fe73,Br77	
1-6	7.8 10^{-2}	4.9 10^{-2}	15.870(4)	15.870(4) Br77 (bl)		
2-10	0.12	0.15	15.870(4)	15.870(4) Br77 (bl)	Fe73, Br77	
1-5	0.34	0.22	16.005(5)	16.005(5) Br77 (bl O VIII)	Fa67,Fe73, Br77	
2-8	5.1 10^{-2}	5.3 10^{-2}	16.026(4)	16.026(4) Br77 (bl)	Fe73, Br77	
3-65	2.9 10^{-3}	4.0 10^{-2}	16.026(4)	16.026(4) Br77 (bl)		
1-4	0.53	0.21	16.072(4)	16.072(4) Br77	Fe73, Br77	
2-7	1.7 10^{-2}	1.4 10^{-2}	16.089(4)	16.087(10) Fe73	Fe73	
3-64	0.15	9.7 10^{-2}	16.166(4)	16.166(4) Br77		
2-5	9.1 10^{-3}	5.8 10^{-3}	16.272(5)	? 16.272(5) Br77	Fe73, Br77	
3-62	4.8 10^{-2}	3.7 10^{-2}	16.306(5)	16.306(5) Br77		Br77
3-29	0.34	0.11	17.622(4)	17.622(4) Ph82		
1-3	4.1	3.4	93.932(9)	93.931(10) Fe73b	Bo70	
2-3	1.5	1.2	103.948(11)	103.954(10) Fe73b	Bo70	
4-14	0.19	2.6 10^{-2}	367.242	? 367.26(20) Dere78		
5-15	0.11	9.0 10^{-3}	405.104	? 405.08 (20) Dere78		
4-12	0.16	1.2 10^{-2}	415.628	? 415.52(20) Dere78		
1-2	4.5	1.1 10^{-5}	974.858(10)	974.86(20) P84	Do75	

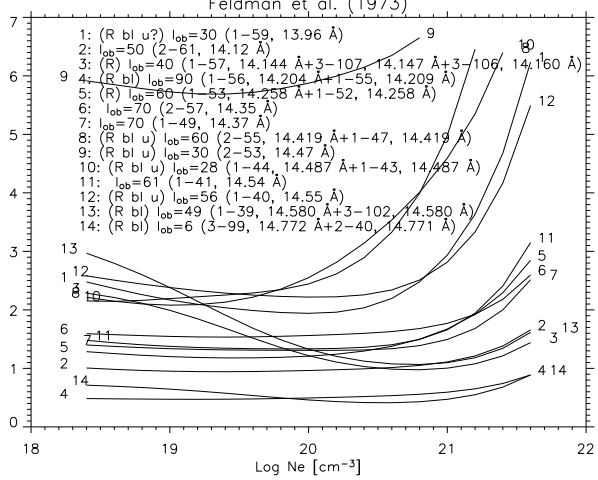

Fig. 1. The emissivity ratio curves (at log T[K]=6.8) relative to the 3d→2p transitions observed by Feldman et al. (1973), where some of the original identifications were proposed. No corrections to the observed intensities are applied. Many lines are obviously blended.

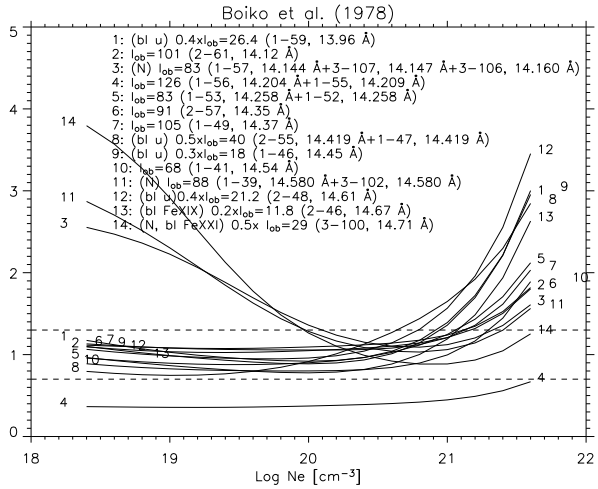

Fig. 2. The emissivity ratio curves (at log T[K]=6.8) relative to the 3d→2p transitions observed in laser spectra by Boiko et al. (1978). The curves show agreement within ±30% (dashed lines).

A similar situation occurs in the case of the SOLEX spectrum by McKenzie et al. (1980), shown in Fig. 6. Only three of the strongest lines appear not to be blended. Most identifications are revised in both cases.

4.1.1. Chandra observations of Capella

The spectral range of the Chandra HETG/MEG spectrometers allows a simultaneous recording of the Fe XVIII $n = 3 \rightarrow 2$ transitions, which can provide some useful temperature diagnostics.

The XUV emission from Capella is nearly isothermal, peaked at 6 MK (see, e.g. Phillips et al. 2001) and therefore the emissivity ratio method should give accurate results. Indeed Desai et al. (2005) found that the Fe XVIII line intensities were, within a few %,

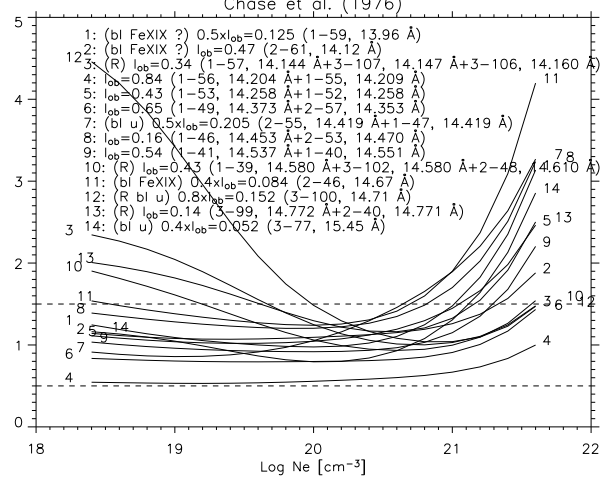

Fig. 3. The emissivity ratio curves (at log T[K]=6.8) relative to the 3d→2p transitions observed in laser spectra by Chase et al. (1976).

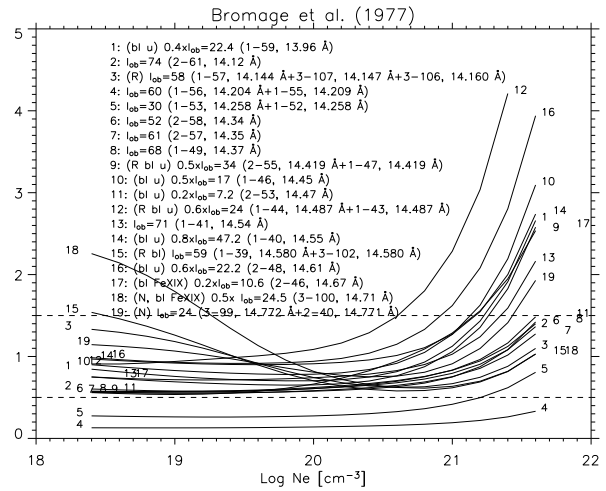

Fig. 4. The emissivity ratio curves (at log T[K]=7.0) relative to the 3d→2p transitions observed in laser spectra by Bromage et al. (1977).

the same when calculated using a full emission measure distribution, or assuming an isothermal one.

A considerable number of papers on Chandra observations of Capella and with substantially different line intensities and identifications (based on various spectral codes or atomic data) can be found in the literature. Surprisingly, the agreement between calculated and observed line intensities is slightly less satisfactory, and strongly depends on which published line intensities are adopted. Two examples are shown here, in Figs. 7,8, based on the tabulations of Phillips et al. (2001) and Desai et al. (2005).

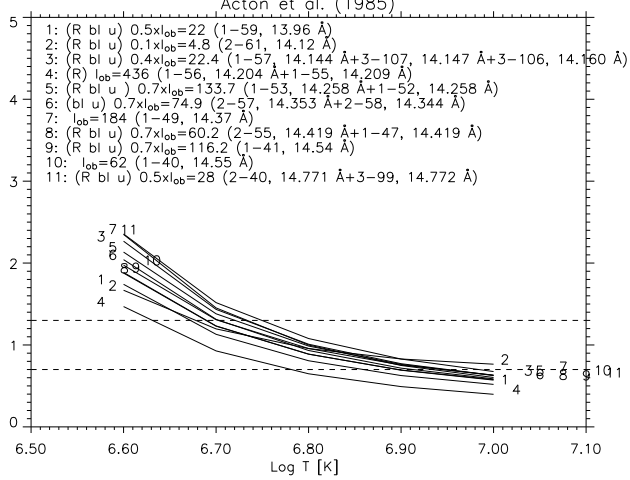

Fig. 5. The emissivity ratio curves relative to the 3d→2p transitions observed in a solar flare spectrum by Acton et al. (1985).

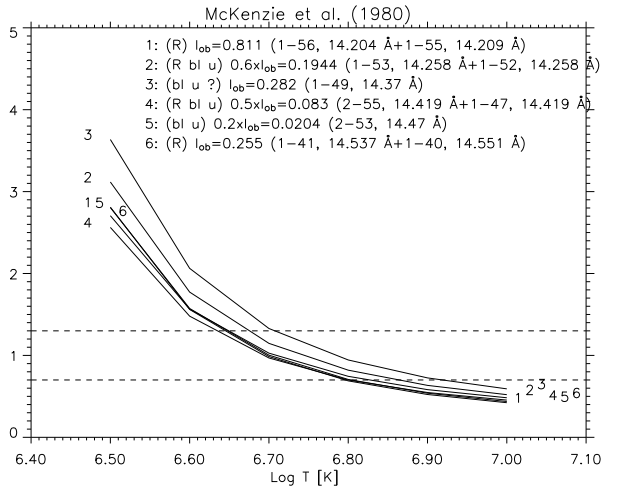

Fig. 6. The emissivity ratio curves relative to the 3d→2p transitions observed with the SOLEX spectrometer by McKenzie et al. (1980).

4.2. 3s→2p and other transitions

$2s^22p^4$ 3s→ $2s^22p$ transitions fall in the 15–17 Å range, and as suggested by Cornille et al. (1995), could be used to measure electron temperatures in astrophysical plasmas. One other positive aspect is that these lines are very strong. As shown in Witthoeft et al (2006), it is only with the latest R-matrix calculations that the theoretical intensities of these lines become similar to the observed ones.

Figs. 9,10,11 present the emissivity ratio curves relative to all the $2s^22p^4$ 3s→ $2s^22p$ brightest transitions observed in the laboratory, solar and stellar plasmas considered in the previous section. Notice that the same scalings as for the 3d→2p transitions has been adopted. The fact that in most cases the curves fall within 30% indicates very good

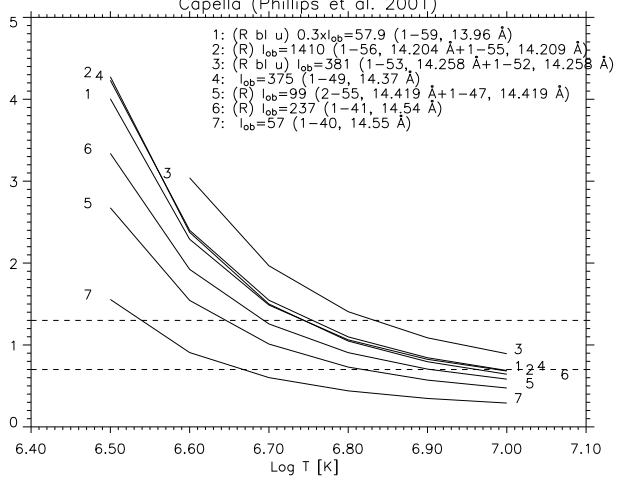

Fig. 7. The emissivity ratio curves relative to the 3d→2p transitions observed in a Chandra spectrum of Capella by Phillips et al. (2001).

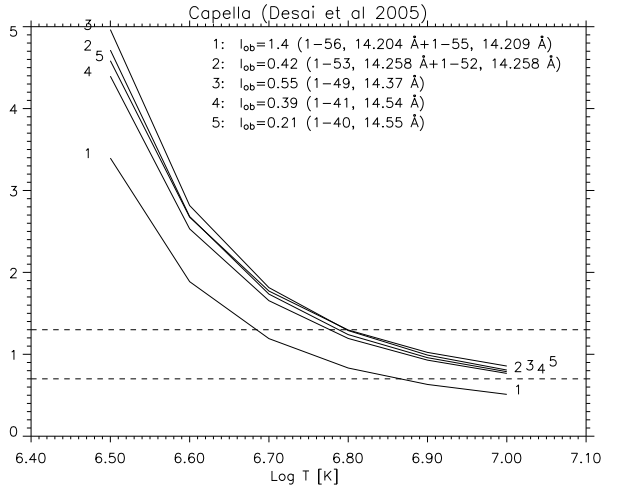

Fig. 8. The emissivity ratio curves relative to the 3d→2p transitions observed in a Chandra spectrum of Capella by Desai et al. (2005).

agreement between the intensities of these two transition arrays. Inspection of the figures also shows the different density/temperature sensitivity of these lines.

Notice that in the majority of cases line identifications have been revised, and blending is present, at different levels depending on the particular observation. Fortunately, there are a few bright lines that consistently appear to be free of blends: the 1-9 $^2P_{3/2}$-$^2D_{5/2}$ at 15.622 Å, the 1-7 $^2P_{3/2}$-$^4P_{3/2}$ at 15.828 Å, the self-blend of the 2-10 $^2P_{1/2}$- $^2D_{3/2}$ and 1-6 $^2P_{3/2}$-$^4P_{1/2}$ transitions at 15.870 Å, the 1-4 $^2P_{3/2}$-$^4P_{5/2}$ at 16.072 Å.

The 1-5 $^2P_{3/2}$-$^2P_{3/2}$ is of particular importance, because, even at the highest spectral resolution, is blended with the Lβ of O VIII, used for diagnostic purposes (cf. Testa et al. 2004). It turns out that in many cases the Fe XVIII contribution to the blend has been underestimated.

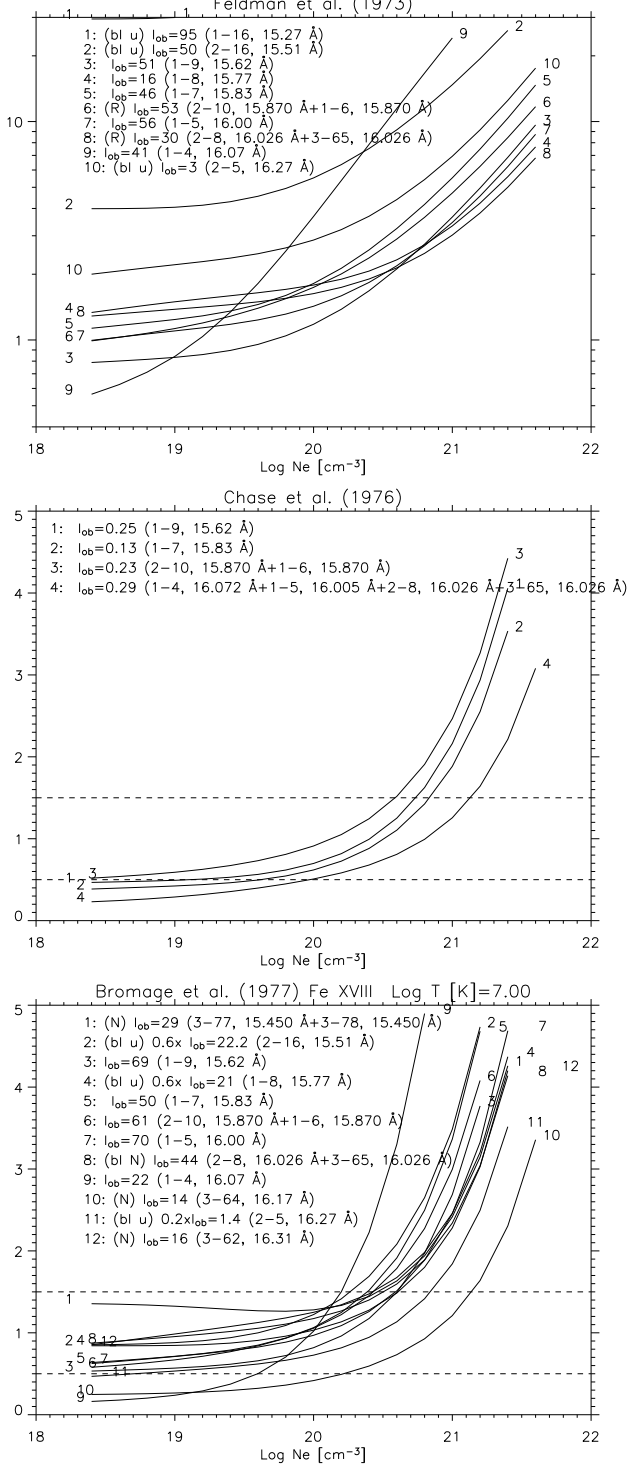

Fig. 9. The emissivity ratio curves (at log T[K]=6.8) relative to the 3s→2p transitions observed by Feldman et al. (1973; no corrections applied), Chase et al. (1976), and Bromage et al. (1977).

The same figures also include a few lines from the $2s^2$ 2p-2s $2p^5$ 3s, 2s $2p^6$-2s $2p^5$ 3s, 2s $2p^6$-$2s^2$ $2p^4$ 3p transition arrays, and that also present good agreement between calculated and observed intensities.

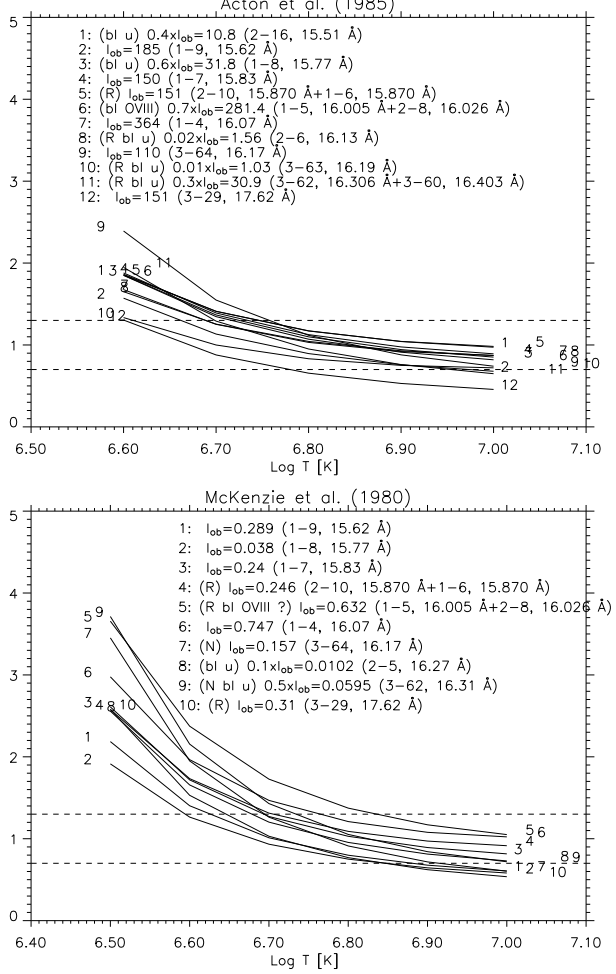

Fig. 10. The emissivity ratio curves relative to the 3s→2p and 3p→2p transitions observed in solar flare spectra by Acton et al. (1985) and McKenzie et al. (1980).

Two strong un-blended lines are worth a particular mention. The 3-64 2s $2p^6$ $^2S_{1/2}$- 2s $2p^5$ 3s $^2P_{3/2}$ at 16.166 Å, and the 3-29 2s $2p^6$ $^2S_{1/2}$- $2s^2$ $2p^4$ 3p $^2P_{3/2}$ at 17.621 Å. Notice that a tentative identification of the latter strong line was proposed by Cornille et al. (1992). SMM and Chandra measurements all consistently indicate a wavelength of 17.621 Å, which provides a firm constraint on the energies of the $2s^2$ $2p^4$ 3p levels. It is interesting to notice that at least three $2s^2$ $2p^4$ 3p → $2s^2$ $2p^4$ 3s lines are predicted to be strong. The corrections to the ab-initio energies provided by the 17.621 Å line suggest three likely matches with (previously unidentified) EUV flare lines in the excellent Skylab spectrum of Dere (1978).

4.2.1. n=2→2 transitions

n=2→2 transitions fall in the EUV spectral range. Contrary to what reported by Desai et al, we find good agreement between the Chandra observations of these lines and the n=3→2 transitions, as Fig. 11 shows.

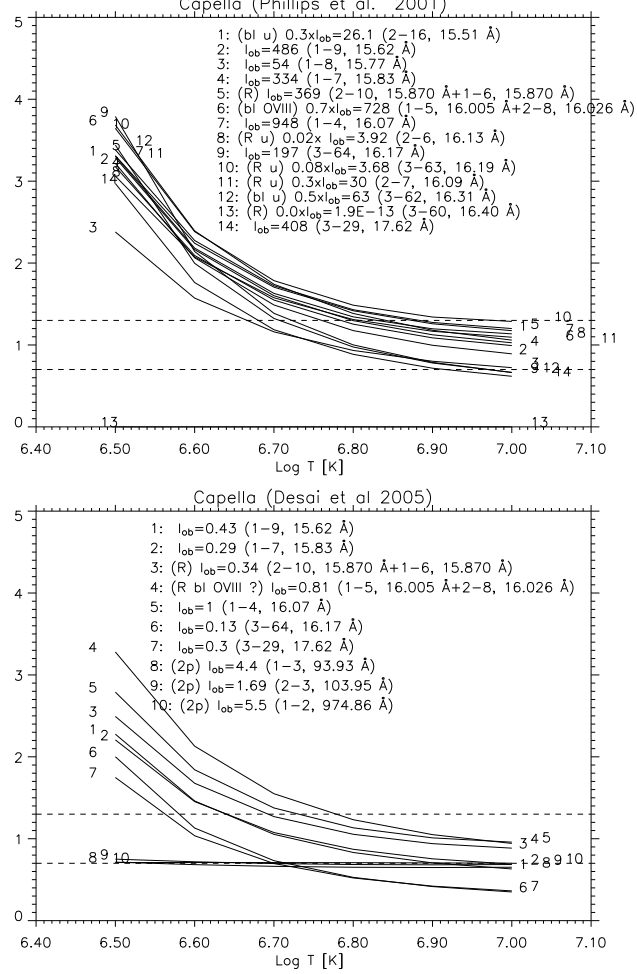

Fig. 11. The emissivity ratio curves relative to the 3s→2p and 3p→2p transitions observed in Chandra spectra of Capella by Phillips et al. (2001) and Desai et al. (2005).

4.2.2. n=4→2 and 2p^5 →3p transitions

In the case of 4d→2p transitions (cf. Fig. 12), the agreement is only marginal, but still acceptable considering the fact that these lines fall in a different spectral range. A similar situation occurs with the 2p^5 →3p transitions (cf. Fig. 13). In the case of 4s→2p transitions no agreement was found.

5. Summary and conclusions

Recent IP R-matrix calculations from Witthoeft et al (2006) have been supplemented with radiative data and used to benchmark Fe XVIII L-shell emission against experimental data.

Good agreement in terms of wavelengths and line intensities is found, thus giving us confidence in the use of these atomic data, which provide intensities for some transitions largely different from those obtained with previous calculations.

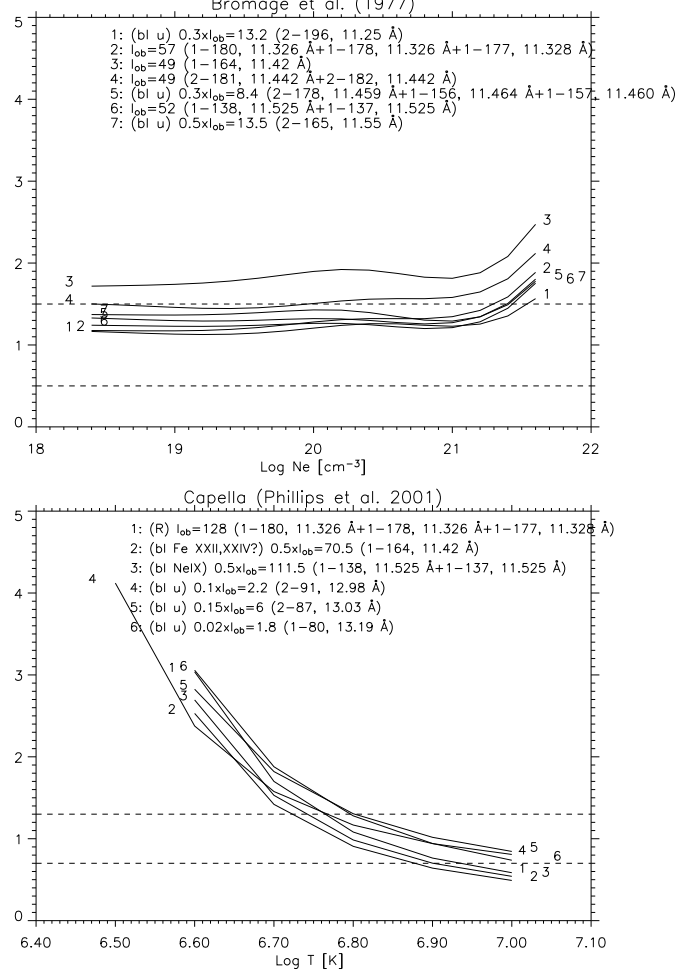

Fig. 12. The emissivity ratio curves relative to the 4d→2p transitions observed by Bromage et al. (1977) and Phillips et al. (2001)

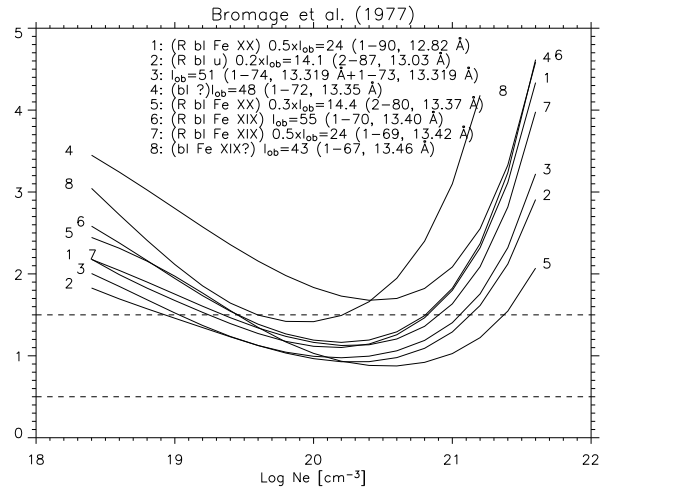

Fig. 13. The emissivity ratio curves relative to the $2p^5$ →3p transitions observed by Bromage et al. (1977).

Most of the previous line identifications found in the literature have been revised on a quantitative basis. In some cases, blends with known transitions were omitted. In

other cases, blends with newly identified lines are suggested. Many lines cannot be due to Fe XVIII and still await firm identification.

It is clear that Fe XVIII L-shell emission can be used to measure electron densities in laboratory plasmas and temperatures for a wide range of 'hot' astrophysical sources. In particular, $n = 3, 4 \rightarrow 2$ transitions are an excellent density diagnostic in laser plasmas. $n = 2, 3 \rightarrow 2$ transitions can be used as temperature diagnostic for solar flare plasmas or stellar coronae, but well-calibrated and high-resolution measurements are required.

Acknowledgements. Support from PPARC (UK) is acknowledged.

References

Acton, L. W., Bruner, M. E., Brown, W. A., et al. 1985, ApJ, 291, 865

Boiko, V. A., Faenov, A. I., & Pikuz, S. A. 1978, Journal of Quantitative Spectroscopy and Radiative Transfer, 19, 11

Boiko, V. A., Voinov, Y., Gribkov, V., & Sklizkov, G. 1970, Opt. and Spectrosc., 29, 1023

Bromage, G. E., Fawcett, B. C., & Cowan, R. D. 1977b, MNRAS, 178, 599

Bromage, G. E., Cowan, R. D., Fawcett, B. C., et al. 1977a, RAL report, 170

Brown, G. V., Beiersdorfer, P., Liedahl, D. A., et al. 2002, ApJS, 140, 589

Buchet, J. P., Buchet-Poulizac, M. C., Denis, A., Désesquelles, J., & Druetta, M. 1980, Phys. Rev. A, 22, 2061

Chase, L. F., Jordan, W. C., Perez, J. D., & Johnston, R. R. 1976, Phys. Rev. A, 13, 1497

Cohen, L., Feldman, U., & Kastner, S. O. 1968, Journal of the Optical Society of America (1917-1983), 58, 331

Cornille, M., Dubau, J., Loulergue, M., Bely-Dubau, F., & Faucher, P. 1992, A&A, 259, 669

Del Zanna, G., Berrington, K. A., & Mason, H. E. 2004, A&A, 422, 731

Del Zanna, G., Chidichimo, M. C., & Mason, H. E. 2005, A&A, 432, 1137

Dere, K. P. 1978, ApJ, 221, 1062

Desai, P., Brickhouse, N. S., Drake, J. J., et al. 2005, ApJ, 625, L59

Doschek, G. A., Dere, K. P., Sandlin, G. D., et al. 1975, ApJ, 196, L83

Eissner, W., Jones, M., & Nussbaumer, H. 1974, Computer Physics Communications, 8, 270

Fawcett, B. C. 1984, Atomic Data and Nuclear Data Tables, 30, 1

Fawcett, B. C., Gabriel, A. H., & Saunders, P. A. H. 1967, Proc. Phys. Soc., 89, 863

Feldman, U., Doschek, G. A., Cowan, R. D., & Cohen, L. 1973a, Journal of the Optical Society of America (1917-1983), 63, 1445

Feldman, U., Doschek, G. A., Nagel, D. J., Behring, W. E., & Cohen, L. 1973b, ApJ, 183, L43+

Kastner, S. O., Neupert, W. M., & Swartz, M. 1974, ApJ, 191, 261

Landi, E., Del Zanna, G., Young, P. R., et al. 2006, ApJS, 162, 261

Landi, E. & Phillips, K. J. H. 2005, ApJS, 160, 286

Mann, J. B. 1983, Atomic Data and Nuclear Data Tables, 29, 407

McKenzie, D. L., Landecker, P. B., Broussard, R. M., et al. 1980, ApJ, 241, 409

McKenzie, D. L., Landecker, P. B., Feldman, U., & Doschek, G. A. 1985, ApJ, 289, 849

Mohan, M., Hibbert, A., Berrington, K. A., & Baluja, K. L. 1987, Journal of Physics B Atomic Molecular Physics, 20, 6319

Neupert, W. M., Gates, W., Swartz, M., & Young, R. 1967, ApJ, 149, L79+

Neupert, W. M., Swartz, M., & Kastner, S. O. 1973, Sol. Phys., 31, 171

Nussbaumer, H. & Storey, P. J. 1978, A&A, 64, 139

Peacock, N. J., Stamp, M. F., & Silver, J. D. 1984, Physica Scripta Volume T, 8, 10

Phillips, K. J. H., Fawcett, B. C., Kent, B. J., et al. 1982, ApJ, 256, 774

Phillips, K. J. H., Mathioudakis, M., Huenemoerder, D. P., et al. 2001, MNRAS, 325, 1500

Sampson, D. H., Zhang, H. L., & Fontes, C. J. 1991, Atomic Data and Nuclear Data Tables, 48, 25

Testa, P., Drake, J. J., Peres, G., & DeLuca, E. E. 2004, ApJ, 609, L79

Witthoeft, M. C., Badnell, N. R., del Zanna, G., Berrington, K. A., & Pelan, J. C. 2006, A&A, 446, 361

Zeippen, C. J., Seaton, M. J., & Morton, D. C. 1977, MNRAS, 181, 527

Table .1. Radiative data for some of the prominent lines.

i-*j*	Terms	gf	A_{ji}	A_{ji} NIST	T	$\lambda_{\rm best}$(Å)	λ(Å) NIST
1-2	$2s^2\ 2p^5\ {}^2P_{3/2}$–$2s^2\ 2p^5\ {}^2P_{1/2}$	-	$1.9\ 10^4$	$1.9\ 10^4$	M1	974.858(10)	974.86
9-20	$2s^2\ 2p^4\ 3s\ {}^2D_{5/2}$–$2s^2\ 2p^4\ 3p\ {}^2P_{3/2}$	$3.0\ 10^{-2}$	$1.3\ 10^8$	-	E1	615.942(22657)	-
1-56	$2s^2\ 2p^5\ {}^2P_{3/2}$–$2s^2\ 2p^4\ 3d\ {}^2D_{5/2}$	3.72	$2.0\ 10^{13}$	-	E1	14.204(2)	14.203
1-4	$2s^2\ 2p^5\ {}^2P_{3/2}$–$2s^2\ 2p^4\ 3s\ {}^4P_{5/2}$	$1.9\ 10^{-2}$	$8.3\ 10^{10}$	$9.1\ 10^{10}$	E1	16.072(4)	16.072
1-55	$2s^2\ 2p^5\ {}^2P_{3/2}$–$2s^2\ 2p^4\ 3d\ {}^2P_{3/2}$	2.35	$1.9\ 10^{13}$	$1.9\ 10^{13}$	E1	14.209(2)	14.203
1-5	$2s^2\ 2p^5\ {}^2P_{3/2}$–$2s^2\ 2p^4\ 3s\ {}^2P_{3/2}$	0.25	$1.6\ 10^{12}$	-	E1	16.005(5)	16.005
1-9	$2s^2\ 2p^5\ {}^2P_{3/2}$–$2s^2\ 2p^4\ 3s\ {}^2D_{5/2}$	0.21	$9.7\ 10^{11}$	$1.1\ 10^{12}$	E1	15.622(3)	15.625
3-29	$2s\ 2p^6\ {}^2S_{1/2}$–$2s^2\ 2p^4\ 3p\ {}^2P_{3/2}$	$7.0\ 10^{-3}$	$3.8\ 10^{10}$	-	E1	17.622(4)	-
1-49	$2s^2\ 2p^5\ {}^2P_{3/2}$–$2s^2\ 2p^4\ 3d\ {}^2D_{5/2}$	1.33	$7.1\ 10^{12}$	-	E1	14.373(2)	14.373
1-41	$2s^2\ 2p^5\ {}^2P_{3/2}$–$2s^2\ 2p^4\ 3d\ {}^2F_{5/2}$	0.82	$4.3\ 10^{12}$	-	E1	14.537(2)	14.534
1-7	$2s^2\ 2p^5\ {}^2P_{3/2}$–$2s^2\ 2p^4\ 3s\ {}^4P_{3/2}$	0.12	$8.0\ 10^{11}$	-	E1	15.828(4)	15.828
1-53	$2s^2\ 2p^5\ {}^2P_{3/2}$–$2s^2\ 2p^4\ 3d\ {}^2S_{1/2}$	0.91	$1.5\ 10^{13}$	$1.6\ 10^{13}$	E1	14.258(2)	14.256
3-64	$2s\ 2p^6\ {}^2S_{1/2}$–$2s\ 2p^5\ 3s\ {}^2P_{3/2}$	0.12	$7.6\ 10^{11}$	-	E1	16.166(4)	16.165
2-10	$2s^2\ 2p^5\ {}^2P_{1/2}$–$2s^2\ 2p^4\ 3s\ {}^2D_{3/2}$	0.18	$1.2\ 10^{12}$	$1.3\ 10^{12}$	E1	15.870(4)	15.870
1-40	$2s^2\ 2p^5\ {}^2P_{3/2}$–$2s^2\ 2p^4\ 3d\ {}^4P_{3/2}$	0.43	$3.4\ 10^{12}$	-	E1	14.551(4)	14.551
2-57	$2s^2\ 2p^5\ {}^2P_{1/2}$–$2s^2\ 2p^4\ 3d\ {}^2D_{3/2}$	1.65	$1.3\ 10^{13}$	$1.5\ 10^{13}$	E1	14.353(8)	14.361
1-164	$2s^2\ 2p^5\ {}^2P_{3/2}$–$2s^2\ 2p^4\ 4d\ {}^2D_{5/2}$	0.60	$5.1\ 10^{12}$	-	E1	11.420(4)	-
1-6	$2s^2\ 2p^5\ {}^2P_{3/2}$–$2s^2\ 2p^4\ 3s\ {}^4P_{1/2}$	$1.3\ 10^{-2}$	$1.8\ 10^{11}$	-	E1	15.870(4)	-
1-138	$2s^2\ 2p^5\ {}^2P_{3/2}$–$2s^2\ 2p^4\ 4d\ {}^2F_{5/2}$	0.54	$4.5\ 10^{12}$	-	E1	11.525(2)	-
1-52	$2s^2\ 2p^5\ {}^2P_{3/2}$–$2s^2\ 2p^4\ 3d\ {}^2F_{5/2}$	0.21	$1.1\ 10^{12}$	-	E1	14.258(2)	-
2-55	$2s^2\ 2p^5\ {}^2P_{1/2}$–$2s^2\ 2p^4\ 3d\ {}^2P_{3/2}$	0.37	$3.0\ 10^{12}$	$3.2\ 10^{12}$	E1	14.419(2)	14.418
2-58	$2s^2\ 2p^5\ {}^2P_{1/2}$–$2s^2\ 2p^4\ 3d\ {}^2P_{1/2}$	1.36	$2.2\ 10^{13}$	-	E1	14.344(6)	14.344
1-47	$2s^2\ 2p^5\ {}^2P_{3/2}$–$2s^2\ 2p^4\ 3d\ {}^4P_{5/2}$	$6.2\ 10^{-2}$	$3.3\ 10^{11}$	-	E1	14.419(2)	-
2-8	$2s^2\ 2p^5\ {}^2P_{1/2}$–$2s^2\ 2p^4\ 3s\ {}^2P_{1/2}$	0.10	$1.3\ 10^{12}$	$1.5\ 10^{12}$	E1	16.026(4)	16.026
1-180	$2s^2\ 2p^5\ {}^2P_{3/2}$–$2s^2\ 2p^4\ 4d\ {}^2D_{5/2}$	0.34	$3.0\ 10^{12}$	-	E1	11.326(4)	-
1-39	$2s^2\ 2p^5\ {}^2P_{3/2}$–$2s^2\ 2p^4\ 3d\ {}^4P_{1/2}$	0.18	$2.8\ 10^{12}$	-	E1	14.580(2)	14.581
3-62	$2s\ 2p^6\ {}^2S_{1/2}$–$2s\ 2p^5\ 3s\ {}^4P_{3/2}$	$7.8\ 10^{-2}$	$4.9\ 10^{11}$	-	E1	16.306(5)	16.305
1-59	$2s^2\ 2p^5\ {}^2P_{3/2}$–$2s^2\ 2p^4\ 3d\ {}^2D_{5/2}$	0.21	$1.2\ 10^{12}$	$1.1\ 10^{12}$	E1	13.962(6)	13.954
1-8	$2s^2\ 2p^5\ {}^2P_{3/2}$–$2s^2\ 2p^4\ 3s\ {}^2P_{1/2}$	$8.6\ 10^{-2}$	$1.2\ 10^{12}$	$1.4\ 10^{12}$	E1	15.766(4)	15.766
1-178	$2s^2\ 2p^5\ {}^2P_{3/2}$–$2s^2\ 2p^4\ 4d\ {}^2P_{3/2}$	0.38	$5.0\ 10^{12}$	-	E1	11.326(4)	-
1-137	$2s^2\ 2p^5\ {}^2P_{3/2}$–$2s^2\ 2p^4\ 4d\ {}^4P_{3/2}$	0.31	$3.9\ 10^{12}$	-	E1	11.525(2)	-
1-70	$2s^2\ 2p^5\ {}^2P_{3/2}$–$2s\ 2p^5\ 3p\ {}^2D_{5/2}$	0.25	$1.6\ 10^{12}$	-	E1	13.397(4)	13.374
1-15	$2s^2\ 2p^5\ {}^2P_{3/2}$–$2s^2\ 2p^4\ 3p\ {}^2D_{5/2}$	-	$1.4\ 10^9$	-	E2	15.397(12)	-
3-99	$2s\ 2p^6\ {}^2S_{1/2}$–$2s\ 2p^5\ 3d\ {}^2D_{3/2}$	0.30	$2.3\ 10^{12}$	-	E1	14.772(4)	-
1-74	$2s^2\ 2p^5\ {}^2P_{3/2}$–$2s\ 2p^5\ 3p\ {}^4P_{5/2}$	0.18	$1.1\ 10^{12}$	-	E1	13.319(6)	-
3-77	$2s\ 2p^6\ {}^2S_{1/2}$–$2s\ 2p^5\ 3s\ {}^2P_{3/2}$	0.13	$8.8\ 10^{11}$	-	E1	15.450(12)	-
1-177	$2s^2\ 2p^5\ {}^2P_{3/2}$–$2s^2\ 2p^4\ 4d\ {}^2S_{1/2}$	0.21	$5.5\ 10^{12}$	-	E1	11.328(6)	-
2-53	$2s^2\ 2p^5\ {}^2P_{1/2}$–$2s^2\ 2p^4\ 3d\ {}^2S_{1/2}$	0.16	$2.5\ 10^{12}$	$2.7\ 10^{12}$	E1	14.470(2)	14.469
1-57	$2s^2\ 2p^5\ {}^2P_{3/2}$–$2s^2\ 2p^4\ 3d\ {}^2D_{3/2}$	0.49	$4.1\ 10^{12}$	$4.3\ 10^{12}$	E1	14.144(8)	14.152
1-46	$2s^2\ 2p^5\ {}^2P_{3/2}$–$2s^2\ 2p^4\ 3d\ {}^2D_{3/2}$	0.13	$1.0\ 10^{12}$	-	E1	14.453(4)	14.453
2-48	$2s^2\ 2p^5\ {}^2P_{1/2}$–$2s^2\ 2p^4\ 3d\ {}^2P_{3/2}$	0.14	$1.1\ 10^{12}$	-	E1	14.610(9)	14.610
3-100	$2s\ 2p^6\ {}^2S_{1/2}$–$2s\ 2p^5\ 3d\ {}^2P_{1/2}$	0.86	$1.3\ 10^{13}$	-	E1	14.706(4)	-
1-72	$2s^2\ 2p^5\ {}^2P_{3/2}$–$2s\ 2p^5\ 3p\ {}^2P_{3/2}$	0.24	$2.2\ 10^{12}$	-	E1	13.355(4)	13.355
1-67	$2s^2\ 2p^5\ {}^2P_{3/2}$–$2s\ 2p^5\ 3p\ {}^4D_{5/2}$	0.10	$6.4\ 10^{11}$	-	E1	13.464(5)	-
1-26	$2s^2\ 2p^5\ {}^2P_{3/2}$–$2s^2\ 2p^4\ 3p\ {}^2F_{7/2}$	-	$9.9\ 10^8$	-	E2	15.010(11)	-
1-69	$2s^2\ 2p^5\ {}^2P_{3/2}$–$2s\ 2p^5\ 3p\ {}^4D_{3/2}$	0.13	$1.2\ 10^{12}$	-	E1	13.424(5)	13.397
2-7	$2s^2\ 2p^5\ {}^2P_{1/2}$–$2s^2\ 2p^4\ 3s\ {}^4P_{3/2}$	$1.1\ 10^{-2}$	$6.9\ 10^{10}$	-	E1	16.089(4)	16.087
2-61	$2s^2\ 2p^5\ {}^2P_{1/2}$–$2s^2\ 2p^4\ 3d\ {}^2D_{3/2}$	1.77	$1.5\ 10^{13}$	$1.5\ 10^{13}$	E1	14.124(2)	14.121
2-16	$2s^2\ 2p^5\ {}^2P_{1/2}$–$2s^2\ 2p^4\ 3s\ {}^2S_{1/2}$	$6.0\ 10^{-2}$	$8.3\ 10^{11}$	$1.1\ 10^{12}$	E1	15.508(4)	15.450
1-90	$2s^2\ 2p^5\ {}^2P_{3/2}$–$2s\ 2p^5\ 3p\ {}^2D_{5/2}$	0.13	$8.6\ 10^{11}$	-	E1	12.818(5)	12.847
1-73	$2s^2\ 2p^5\ {}^2P_{3/2}$–$2s\ 2p^5\ 3p\ {}^2P_{1/2}$	0.18	$3.3\ 10^{12}$	-	E1	13.319(6)	-
1-58	$2s^2\ 2p^5\ {}^2P_{3/2}$–$2s^2\ 2p^4\ 3d\ {}^2P_{1/2}$	0.27	$4.4\ 10^{12}$	-	E1	14.136(6)	-
3-102	$2s\ 2p^6\ {}^2S_{1/2}$–$2s\ 2p^5\ 3d\ {}^2P_{3/2}$	1.90	$1.5\ 10^{13}$	-	E1	14.580(2)	-
3-107	$2s\ 2p^6\ {}^2S_{1/2}$–$2s\ 2p^5\ 3d\ {}^2D_{3/2}$	0.32	$2.7\ 10^{12}$	-	E1	14.147(10)	-
1-42	$2s^2\ 2p^5\ {}^2P_{3/2}$–$2s^2\ 2p^4\ 3d\ {}^2P_{1/2}$	$1.3\ 10^{-2}$	$2.1\ 10^{11}$	-	E1	14.499(11)	14.486
2-182	$2s^2\ 2p^5\ {}^2P_{1/2}$–$2s^2\ 2p^4\ 4d\ {}^2P_{1/2}$	0.35	$8.8\ 10^{12}$	-	E1	11.442(2)	-
2-75	$2s^2\ 2p^5\ {}^2P_{1/2}$–$2s\ 2p^5\ 3p\ {}^4P_{3/2}$	$7.2\ 10^{-2}$	$6.6\ 10^{11}$	-	E1	13.493(9)	13.464
2-165	$2s^2\ 2p^5\ {}^2P_{1/2}$–$2s^2\ 2p^4\ 4d\ {}^2P_{3/2}$	0.23	$2.9\ 10^{12}$	-	E1	11.551(5)	11.551
3-105	$2s\ 2p^6\ {}^2S_{1/2}$–$2s\ 2p^5\ 3d\ {}^2P_{3/2}$	1.69	$1.4\ 10^{13}$	-	E1	14.177(10)	-
2-87	$2s^2\ 2p^5\ {}^2P_{1/2}$–$2s\ 2p^5\ 3p\ {}^2D_{3/2}$	0.12	$1.2\ 10^{12}$	-	E1	13.034(8)	13.049
2-80	$2s^2\ 2p^5\ {}^2P_{1/2}$–$2s\ 2p^5\ 3p\ {}^2S_{1/2}$	0.17	$3.2\ 10^{12}$	-	E1	13.374(9)	13.355
3-65	$2s\ 2p^6\ {}^2S_{1/2}$–$2s\ 2p^5\ 3s\ {}^2P_{1/2}$	0.11	$1.4\ 10^{12}$	-	E1	16.026(4)	-
2-196	$2s^2\ 2p^5\ {}^2P_{1/2}$–$2s^2\ 2p^4\ 4d\ {}^2D_{3/2}$	0.28	$3.7\ 10^{12}$	-	E1	11.253(4)	11.253
2-79	$2s^2\ 2p^5\ {}^2P_{1/2}$–$2s\ 2p^5\ 3p\ {}^2D_{3/2}$	0.18	$1.6\ 10^{12}$	-	E1	13.412(9)	13.397
3-78	$2s\ 2p^6\ {}^2S_{1/2}$–$2s\ 2p^5\ 3s\ {}^2P_{1/2}$	$2.7\ 10^{-2}$	$3.8\ 10^{11}$	-	E1	15.450(12)	-
1-3	$2s^2\ 2p^5\ {}^2P_{3/2}$–$2s\ 2p^6\ {}^2S_{1/2}$	0.21	$8.1\ 10^{10}$	$9.1\ 10^{10}$	E1	93.932(9)	93.926
2-3	$2s^2\ 2p^5\ {}^2P_{1/2}$–$2s\ 2p^6\ {}^2S_{1/2}$	$9.6\ 10^{-2}$	$3.0\ 10^{10}$	$3.3\ 10^{10}$	E1	103.948(11)	103.939
4-14	$2s^2\ 2p^4\ 3s\ {}^4P_{5/2}$–$2s^2\ 2p^4\ 3p\ {}^4D_{7/2}$	0.82	$5.1\ 10^9$	-	E1	367.242(8626)	-
4-12	$2s^2\ 2p^4\ 3s\ {}^4P_{5/2}$–$2s^2\ 2p^4\ 3p\ {}^4P_{5/2}$	0.50	$3.2\ 10^9$	-	E1	415.628(11015)	-
5-15	$2s^2\ 2p^4\ 3s\ {}^2P_{3/2}$–$2s^2\ 2p^4\ 3p\ {}^2D_{5/2}$	0.55	$3.7\ 10^9$	-	E1	405.104(11093)	-